2008 IEEE International Conference on
Robotics and Automation
Pasadena, CA, USA, May 19-23, 2008

Influence of Internal Vibration Modes on the Stability of Haptic Rendering

Iñaki Díaz, *Student, IEEE*, and Jorge Juan Gil, *Member, IEEE*

***Abstract*— Developing stable controllers able to exhibit a wide dynamic range of impedances is a persistent challenge in the field of haptics. This paper addresses the effect of internal vibration modes on the stability boundary for haptic rendering. A theoretical study that analyzes the influence of the first resonant mode on the maximum achievable impedance is presented. Experiments carried out on the LHIfAM haptic interface support the theoretical conclusions. A control architecture that overcomes the undesired effect of the resonant mode on the stability is also described.**

***Index Terms*— Haptic systems, Stability, Vibrations**

I. Introduction

Over the past years haptic interfaces have been successfully integrated into a wide range of fields such as engineering [1] or surgery [2], [3]. Haptic devices allow users to interact with a certain environment, either remote or virtual, by the sense of touch. In these applications—unlike in conventional robotic systems—the user shares workspace with the device. Therefore, an unstable behavior can damage the device, or even worse, harm the operator. Thus, stability must be guaranteed to ensure user safety and achieve high haptic performance. Unfortunately, preserving haptic stability usually implies reducing the range of dynamic impedances achievable by the system. Hence, rigid virtual objects cannot be perceived as stiff as real ones, and the overall haptic performance is considerably degraded.

In a haptic system, the critical impedance depends on many factors, such as inherent interface dynamics, motor saturation, sensor resolution or time delay. Several studies [4], [5], [6], have previously analyzed how these phenomena affect the stability and passivity boundary. However, the mathematical models used to analyze stability rarely take into account the existence of internal vibration modes. This paper presents a theoretical approach that studies the influence of internal vibration modes on the stability of haptic rendering. In particular, it addresses the influence of the first resonant mode of cable transmission used in haptic devices. This type of mechanical transmissions is widely used in haptic devices because it offers a number of advantages such as low friction, no backlash and low weight [7]. Well-known haptic devices—i.e. the PHANToM haptic interface—use this type of transmission.

This work has been supported in part by the Basque Government, project number S-PE05TE01.

I. Díaz and J. J. Gil are with the Applied Mechanics Department, CEIT, Paseo Manuel Lardizábal 15, E-20018 San Sebastián, Spain (phone: +34 943 212 800; fax: +34 943 213 076; e-mails: {idiaz,jjgil}@ceit.es) and the Control and Electronics Department, TECNUN, University of Navarra, Paseo Manuel Lardizábal 13, E-20018 San Sebastián, Spain.

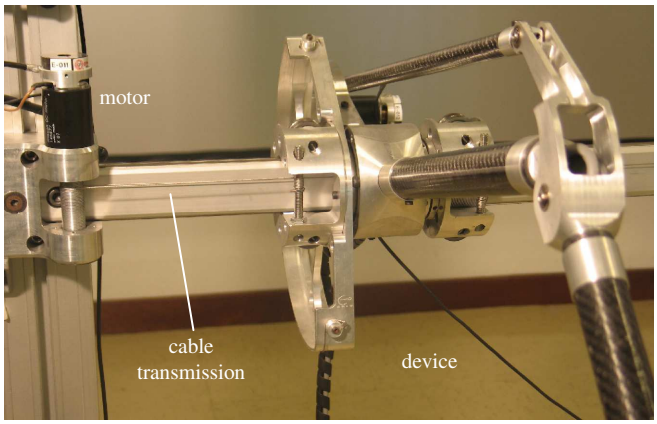

Fig. 1. Cable transmission of the translational degree-of-freedom of the LHIfAM haptic interface.

The paper is organized as follows: in Section II a haptic model with a single vibration mode is presented. Section III theoretically analyzes the stability of the system using an impedance interaction with the virtual environment. Section IV shows the influence of the first resonant mode on the gain margin of the system, and Section V supports the analytical study with experiments carried out on the LHIfAM haptic interface [8], [9] (Fig. 1). Section VI presents an alternative control architecture for the system, and final conclusions are summarized in Section VII.

II. System Description

Fig. 2(a) illustrates a simplified model commonly used to analyze the stability of haptic systems [10], [6]. It has a mass m and a viscous damping b, and the model assumes that the mechanical device is perfectly rigid. Although the force exerted by the motor F_m and the force exerted by the user F_h are introduced in different places, a single transfer function is defined for this model,

$$X_h = G(s)(F_h + F_m), \tag{1}$$

which is

$$G(s) = \frac{1}{ms^2 + bs}. \tag{2}$$

However, several authors [11], [12], have remarked the existence of internal vibration modes in haptic devices. Fig. 2(b) shows a haptic system with a single vibration mode. The terminology used is defined for the case in which the vibration mode is that of the cable transmission connecting the motor (subscript m) and the main body of the device (subscript d). The dynamic properties of the cable are

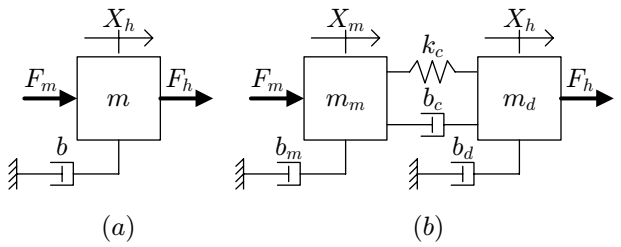

Fig. 2. Scheme of a perfectly rigid haptic device (a), and haptic device with a single vibration mode (b).

TABLE I
PHYSICAL PARAMETERS OF THE LHIfAM

Parameter	Variable	Value
Mass	m	5.4 kg
Motor mass	m_m	0.3 kg
Body mass	m_d	5.1 kg
Damping	b	3.5 Ns/m
Motor damping	b_m	0.1 Ns/m
Body damping	b_d	3.4 Ns/m
Cable stiffness	k_c	79.5 kN/m
Cable damping	b_c	15 Ns/m

characterized by a spring and a damper, with coefficients k_c and b_c respectively.

The new model is a two-input/two-output system. The relationship between output positions and input forces is

$$\begin{bmatrix} X_h \\ X_m \end{bmatrix} = \begin{bmatrix} G_d(s) & G_c(s) \\ G_c(s) & G_m(s) \end{bmatrix} \begin{bmatrix} F_h \\ F_m \end{bmatrix}, \tag{3}$$

or,

$$\mathbf{x} = \mathbf{G}\mathbf{f}. \tag{4}$$

Three new transfer functions have been defined,

$$G_d(s) = \frac{p_m(s)}{p_d(s)p_m(s) - (k_c + b_c s)^2}, \tag{5}$$

$$G_c(s) = \frac{k_c + b_c s}{p_d(s)p_m(s) - (k_c + b_c s)^2}, \tag{6}$$

$$G_m(s) = \frac{p_d(s)}{p_d(s)p_m(s) - (k_c + b_c s)^2}, \tag{7}$$

where,

$$p_d(s) = m_d s^2 + (b_d + b_c)s + k_c, \tag{8}$$

$$p_m(s) = m_m s^2 + (b_m + b_c)s + k_c. \tag{9}$$

As can be expected, all these transfer functions have the same characteristic equation. Fig. 3 shows the Bode diagrams of $G_d(s)$, $G_c(s)$ and $G_m(s)$ calculated with the physical parameters of the translational degree-of-freedom of the LHIfAM, shown in Table I.

An experimental approach described in [11] has been followed in order to obtain the dynamic properties of the cable (k_c and b_c). Before the experiment, the position of the haptic device is mechanically locked. Then, a swept sine wave input that varies from 10 to 200 Hz is applied to the motor, and the output position response is measured. Parameters are fitted from the relationship between the frequency content of input and output signals. Fig. 4 shows both the experimental and

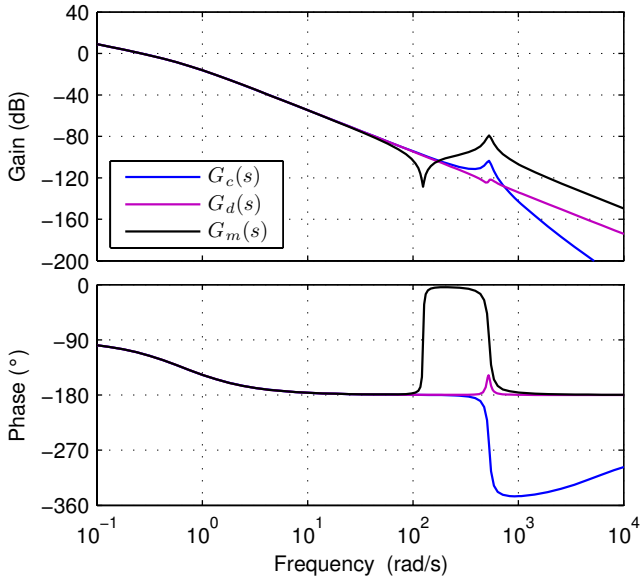

Fig. 3. Bode diagrams of $G_d(s)$, $G_c(s)$ and $G_m(s)$ calculated for the LHIfAM.

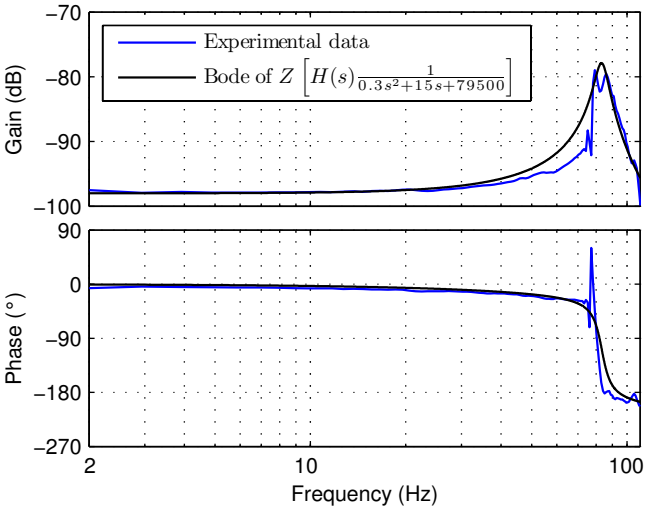

Fig. 4. Frequency response of the system to a chirp force input (blue) and Bode diagram of the cable model (black) after parameter fitting.

empirically modeled results after parameter fitting. Although the cable stiffness may be nonlinear (i.e. dependent on position), the figure shows that a spring-damper model is valid to adequately characterize the dynamic behavior of the cable.

Assuming that $m = m_m + m_d$ and $b = b_m + b_d$, an alternative way to define the system is

$$\mathbf{G} = G(s)\frac{\omega_n^2}{s^2 + z_n s + \omega_n^2}\begin{bmatrix} \frac{s^2+z_1 s+\omega_1^2}{\omega_1^2} & 1 + \frac{b_c}{k_c}s \\ 1 + \frac{b_c}{k_c}s & \frac{s^2+z_2 s+\omega_2^2}{\omega_2^2} \end{bmatrix} \tag{10}$$

where,

$$\omega_1^2 = \frac{k_c}{m_m}, \tag{11}$$

$$\omega_2^2 = \frac{k_c}{m_d}, \tag{12}$$

$$\omega_n^2 = \frac{k_c m}{m_d m_m}, \tag{13}$$

$$z_1 = \frac{b_m + b_c}{m_m}, \tag{14}$$

$$z_2 = \frac{b_d + b_c}{m_d}, \tag{15}$$

$$z_n = z_1 + z_2 - \frac{b}{m}. \tag{16}$$

This formulation shows that the original transfer function $G(s)$ remains valid at low frequencies, because the other elements add 0 dB and 0° within that range. The vibration mode is characterized by the underdamped second-order transfer function whose natural frequency is ω_n.

III. Impedance Interaction

Introducing an impedance interaction with the virtual environment, the device can be analyzed as a single-input/single-output system, as it is illustrated in Fig. 5. $C(z)$ is the force model of the virtual contact (which usually includes a spring and a damper) and $H(s)$ is the zero-order-holder. T is the sampling period.

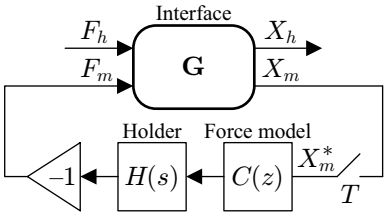

Fig. 5. Haptic system with impedance interaction.

Using (3) and force model

$$F_m(s) = -H(s)C(z)X_m^*(s), \tag{17}$$

the output positions are

$$X_h(s) = G_d(s)F_h(s) - G_c(s)H(s)C(z)X_m^*(s), \tag{18}$$

$$X_m(s) = G_c(s)F_h(s) - G_m(s)H(s)C(z)X_m^*(s), \tag{19}$$

and the sampled position of the motor is given by

$$X_m^*(s) = \frac{Z[G_c(s)F_h(s)]}{1 + C(z)Z[H(s)G_m(s)]}. \tag{20}$$

A possible way to depict the block diagram of the single-input/single-output system—using (18) and (19)—is shown in Fig. 6.

The stability of the haptic system with impedance interaction depends on the position of the poles of the following characteristic equation,

$$1 + C(z)Z[H(s)G_m(s)] = 0. \tag{21}$$

If the force model has a virtual spring with stiffness K, the characteristic equation becomes

$$1 + KZ[H(s)G_m(s)] = 0, \tag{22}$$

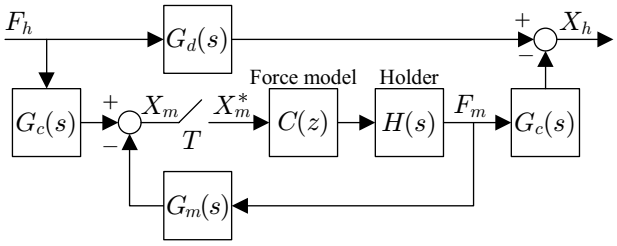

Fig. 6. Block diagram of the system with impedance interaction.

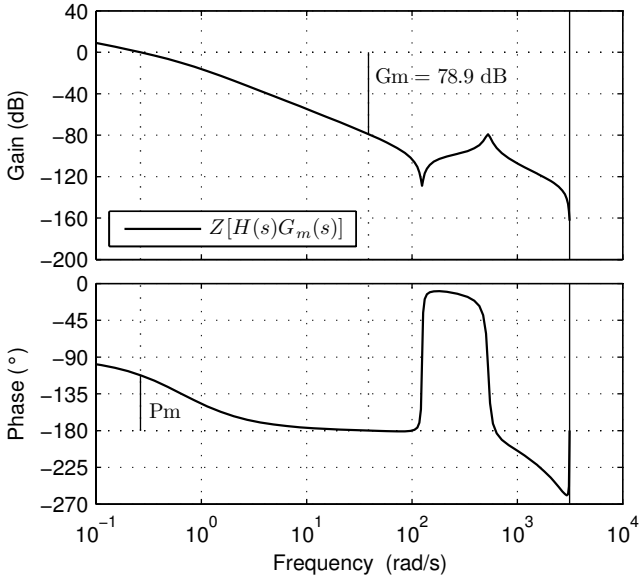

Fig. 7. Bode diagram and margins of $Z[H(s)G_m(s)]$ calculated for the LHIfAM.

and the critical stiffness is

$$K_{CR} = \text{Gm}\{Z[H(s)G_m(s)]\}, \tag{23}$$

where Gm{.} means gain margin of the transfer function within brackets.

Fig. 7 shows the Bode diagram of $Z[H(s)G_m(s)]$ for the LHIfAM. It can be observed that the magnitude of the gain margin, and the frequency at which it is placed, are not being influenced by the resonant peak caused by the vibration mode. Since $G(s)$ and $G_m(s)$ are similar at those frequencies, the vibration mode does not have to be considered to obtain the stability boundary. In other words, $G(s)$ is good enough to characterize the systems. And previous stability criteria [6] that do not consider the influence of vibration modes in the system are adequate to calculate the critical stiffness of the system.

IV. Influence of the Vibration Mode

The theoretical analysis of Section III has shown that the resonant mode of the cable transmission of the LHIfAM does not affect the stability boundary. However, it is also evident from Fig. 7 that the resonant peak could easily impose the stability margin.

We have decreased the initial pretension of the cable in order to analyze how this affects the stability of the system.

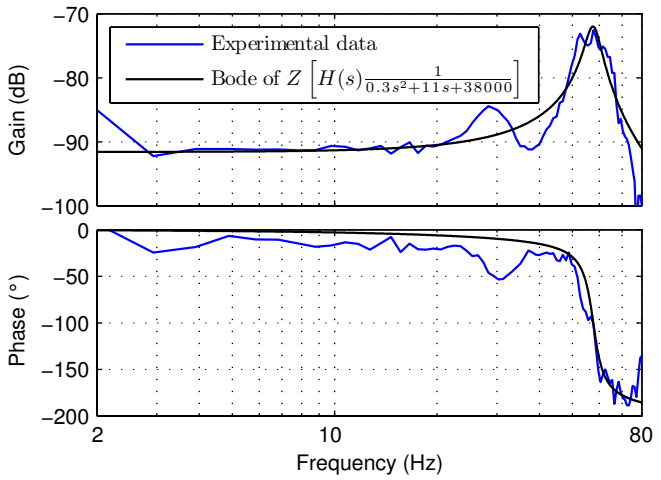

Fig. 8. Frequency response of the system to a chirp force input (blue) and Bode diagram of the cable model (black) with decreased pretension.

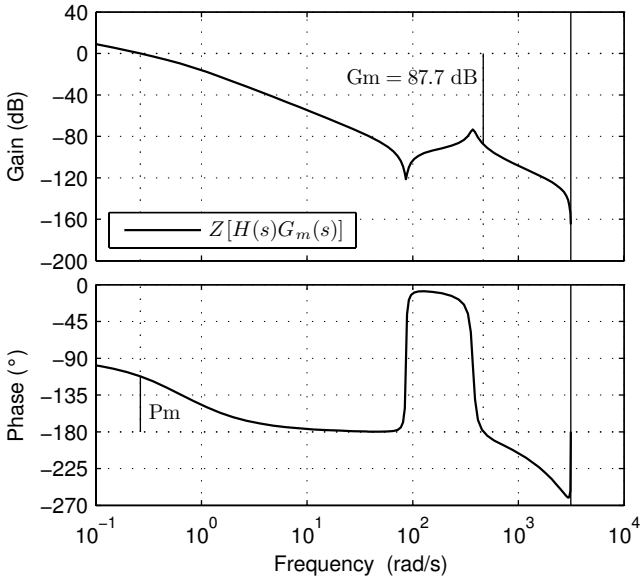

Fig. 9. Bode diagram and margins of $Z[H(s)G_m(s)]$ calculated for the LHIfAM after reducing cable pretension.

Fig. 8 presents the new dynamic properties of the cable transmission.

Fig. 9 shows the Bode diagram of $Z[H(s)G_m(s)]$ for the new cable transmission setup. In this case, the first resonant mode of the cable does impose the gain margin of the system. Notice that the new gain margin is larger than the one of the original system, but placed at a higher frequency. Although it may not seem evident in Fig. 9, there is only one phase crossover frequency at 411.23 rad/s in the Bode diagram.

A possible criterion to estimate whether the resonant peak does influence on the critical stiffness is to measure the distance Q from the resonant peak to 0 dB. This distance is approximately

$$Q \approx m_m z_n \omega_n. \tag{24}$$

Distance Q should be compared with the critical stiffness obtained using the criterion presented in [6], which gives a gain margin similar to the one shown in Fig. 7. If Q is similar or larger than that value, then the vibration mode should be taken into account in the stability analysis. Using the parameters of the LHIfAM, Q is approximately 78.16 dB (with original cable setup).

V. Experimental Results

The translational degree-of-freedom of the LHIfAM haptic interface (Fig. 1) has been used as testbed to perform experiments. The device is controlled by a dSPACE DS1104 board that reads encoder information, processes the haptic control loop and outputs torque commands to the motor at a sampling rate of 1 kHz. The linear transmission provides a 1500 mm linear stroke and a resolution of 3.14 μm with a QuantumDevices D145 encoder. Cable transmission is driven by a commercial Maxon RE40 dc motor. Experiments were performed after reducing cable pretension (Fig. 8).

An interesting approach is to experimentally seek out—by tuning a controllable parameter in the same system—several critical stiffness values K_{CR}: some that are influenced by the resonant frequency and others that are not. This can be achieved by introducing an elastic force model with different time delays t_d:

$$C(z) = Kz^{-\frac{t_d}{T}}. \tag{25}$$

This way, the characteristic equation becomes

$$1 + Kz^{-\frac{t_d}{T}} Z[H(s)G_m(s)] = 0, \tag{26}$$

and the critical stiffness is

$$K_{CR} = \text{Gm}\{z^{-\frac{t_d}{T}} Z[H(s)G_m(s)]\}, \tag{27}$$

$$K_{CR} = \text{Gm}\{Z[H(s)G_m(s)e^{-t_d s}]\}. \tag{28}$$

Without any delay in the system, the gain margin should be imposed by the resonant peak of the vibration mode. Introducing certain time delays within the loop the gain margin should move to the linear region of the Bode where the slope is -40 dB/decade (as it is schematically shown in Fig. 10).

The critical virtual stiffness of the device is calculated by means of the relay experiment described in [13], [10], [14], with and without time delay. In this experiment a relay feedback—an on-off controller—makes the system oscillate around a reference position. In steady state, the input force is a square wave, the output position is similar to a sinusoid wave, and both have opposite phase. These two signals in opposite phase are shown in Fig. 11.

It can be demonstrated [13] that the ultimate frequency is the oscillation frequency of both signals, and the ultimate gain is the quotient of the amplitudes of the first harmonic of the square wave and the output position. This ultimate gain is, of course, the critical gain of this system. Since we are relating force exerted on the interface and position, this critical gain is precisely the maximum achievable virtual stiffness for stability.

Nine trials with varying delays in the input force (from 0 to 8 ms) were performed. Each one of these trials was

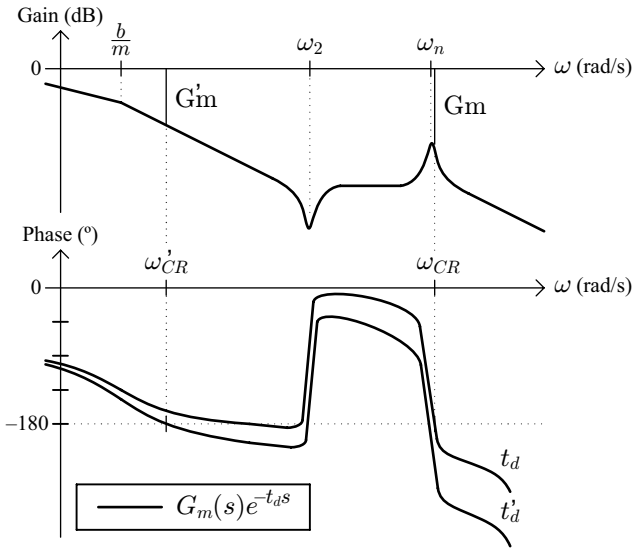

Fig. 10. Scheme of the Bode diagram of $G_m(s)e^{-t_d s}$ for two different time delays ($t_d < t'_d$).

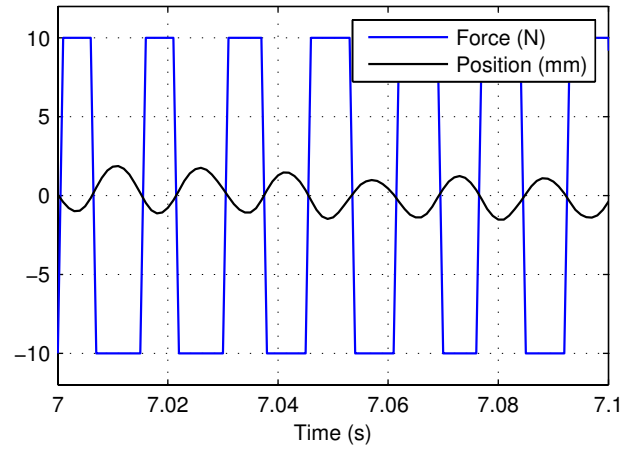

Fig. 11. Force input and position output of a relay experiment for time delay $t_d = 0$.

TABLE II

CRITICAL OSCILLATIONS OF THE LHIfAM

t_d (ms)	ω_{CR} (Hz)	Gm (dB)	t_d (ms)	ω_{CR} (Hz)	Gm (dB)
0	64.9414	80.3149	4	4.5166	73.9436
0	64.4531	79.9414	4	4.6387	74.6716
0	65.4297	80.3552	5	4.5166	73.9604
0	65.4297	80.3019	5	4.3945	73.6567
1	60.0586	76.2336	5	4.3945	73.4947
1	59.0820	75.3235	5	4.3945	73.3171
1	60.3027	75.8445	6	3.1738	66.8281
1	58.9600	75.3917	6	3.1738	66.7290
2	4.8828	76.1063	6	3.1738	66.6668
2	4.8828	76.4240	6	3.1738	66.7219
2	4.8828	76.9967	7	2.8076	64.1974
2	4.8828	75.7971	7	2.8076	64.4480
3	4.3945	73.5975	7	2.6855	64.1268
3	4.3945	73.8443	7	2.8076	64.6013
3	4.3945	72.9533	8	2.3193	61.0258
3	4.3945	73.9426	8	2.3193	60.8367
4	4.3945	73.5919	8	2.3193	61.3209
4	4.3945	73.6444	8	2.3193	61.4755

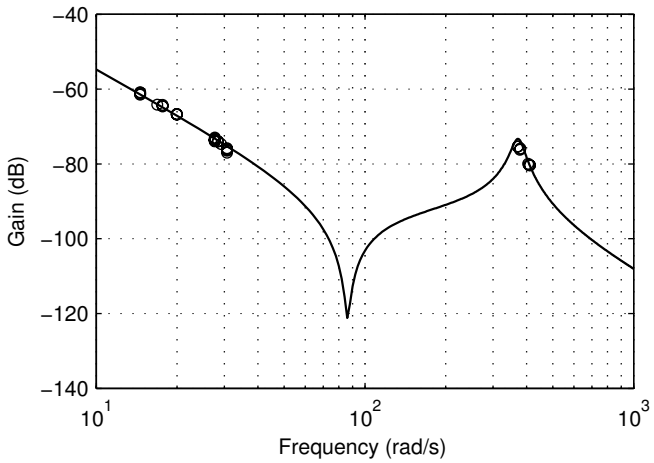

Fig. 12. Experimental gain margins obtained for several time delays by the relay experiment (circles), and the Bode diagram of $Z[H(s)G_m(s)]$ calculated for the LHIfAM (line).

repeated four times in order to have consistent data for further analysis, and in each experiment input-output data values were measured for more than 15 seconds (in steady state). Oscillation frequencies were found by determining the maximum peak of the average power spectral density of both signals. Gain margins were obtained by evaluating the estimated empirical transfer function at that frequency. Table II presents these oscillation frequencies and gain margins.

Fig. 12 shows that results of Table II and the Bode diagram of $Z[H(s)G_m(s)]$ calculated for the LHIfAM match properly. Notice that the resonant peak of the vibration mode conditions the stability of the system only for short delays. All these experiments confirm the theoretical conclusions of Section IV.

Critical gain margins shown in Table II for the undelayed system should be similar to the gain margin obtained theoretically in Fig. 9. However, they differ in more than 7 dB. A possible reason could be that most practical systems experience some amplifier and computational delay in addition to the effective delay of the zero-order holder [5]. This inherit delay has been estimated using the Bode diagram of Fig. 9, and is approximately 250 μs.

VI. ALTERNATIVE SYSTEM ARCHITECTURE

The gain margin and the critical stiffness of the system could not be affected by the vibration mode of the cable transmission if the feedback loop uses the position of the user instead of the position of the motor. Fig. 13 presents two equivalent block diagrams of this architecture.

With this architecture, the sampled position of the user becomes

$$X_h^*(s) = \frac{Z[G_d(s)F_h(s)]}{1 + C(z)Z[H(s)G_c(s)]}, \qquad (29)$$

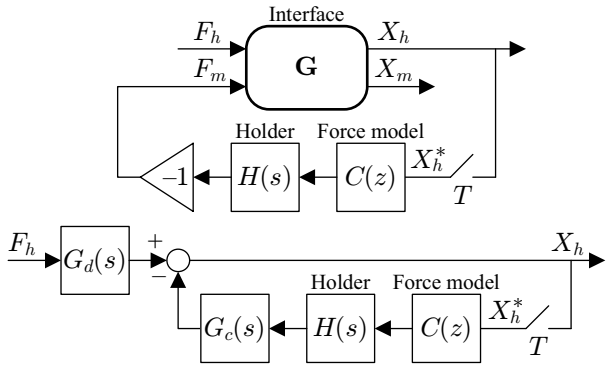

Fig. 13. Equivalent block diagrams of the alternative architecture.

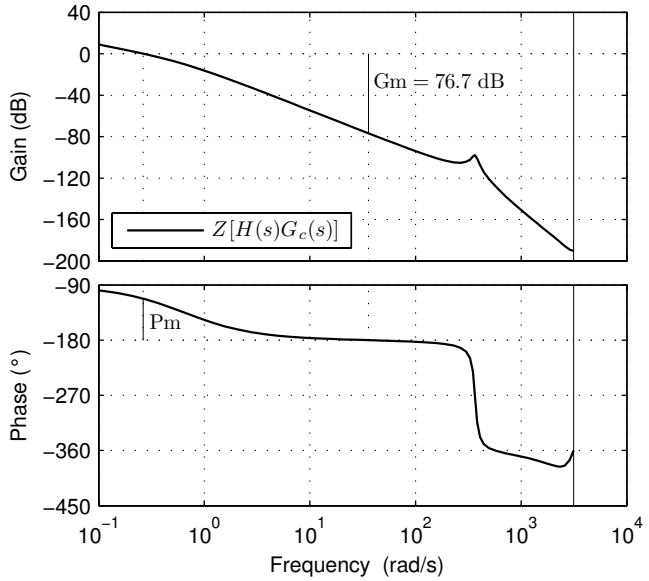

Fig. 14. Bode diagram and margin of $Z[H(s)G_c(s)]$ computed with the parameters of the LHIfAM.

and using an elastic force model, the critical stiffness is

$$K_{CR} = \text{Gm}\{Z[H(s)G_c(s)]\}. \tag{30}$$

The Bode diagram presented in Fig. 14 shows that in this case the vibration mode does not play any role in the gain margin of the system. The plot has been depicted by using the parameters of the LHIfAM with the cable pretension of Section IV.

Despite the advantages of the control strategy described in this section, accurately measuring user position is not clear-cut and requires the modification of the current configuration of our system. In future research, we plan to perform experiments to verify the benefits of the proposed approach.

VII. Conclusions

This paper has examined the influence of internal vibration modes on the stability of haptic rendering. Haptic models commonly used to analyze stability rarely take into account this phenomenon. This work shows that the first resonant mode of cable transmissions used in haptic interfaces can affect the stability boundary for haptic rendering. A criterion that estimates when this fact occurs is presented. Experiments carried out on a haptic interface support the theoretical conclusions.

The main dynamic properties of the cable transmission of our haptic interface have been modeled experimentally. The identification of the first vibration mode has been proven enough to adequately characterize the transmission and obtain the critical stiffness of the system.

An alternative control architecture that overcomes the undesired effect of the resonant mode has also been presented. In future work, we plan to experimentally verify the benefits and drawbacks of this strategy.

Human operator dynamics does modify the stability margins presented in this paper. It has already been shown [10], [15] that human operator tends to stabilize the system for the rigid model presented in Fig. 2(a). Therefore, the control scheme without its influence can be considered as the worst case for stability. Further work will also analyze this fact for the case of the model including the vibration mode.

References

[1] E. Chen, "Six degree-of-freedom haptic system for desktop virtual prototyping applications," in *First International Workshop on Virtual Reality and Prototyping*, Laval, France, 1999, pp. 97–106.

[2] A. J. Madhani, G. Niemeyer, and J. K. Salisbury, "The black falcon: A teleoperated surgical instrument for minimally invasive surgery," in *IEEE/RSJ Int. Conf. Intell. Robot. Syst.*, Victoria B.C., Canada, 1998, pp. 936–944.

[3] M. Li and Y.-H. Liu, "Haptic modeling and experimental validation for interactive endodontic simulation," in *IEEE Int. Conf. Robot. Autom.*, Orlando, Florida, USA, 2006, pp. 3292–3297.

[4] J. J. Abbott and A. M. Okamura, "Effects of position quantization and sampling rate on virtual-wall passivity," *IEEE Trans. Robot.*, vol. 21, no. 5, pp. 952–964, 2005.

[5] N. Diolaiti, G. Niemeyer, F. Barbagli, and J. K. Salisbury, "Stability of haptic rendering: Discretization, quantization, time-delay and coulomb effects," *IEEE Trans. Robot.*, vol. 22, no. 2, pp. 256–268, 2006.

[6] J. J. Gil, E. J. Sánchez, T. Hulin, C. Preusche, and G. Hirzinger, "Stability boundary for haptic rendering: Influence of damping and delay," in *IEEE Int. Conf. Robot. Autom.*, Roma, Italy, 2007, pp. 124–129.

[7] W. T. Townsend, "The effect of transmission design on force-controlled manipulator performance," Ph.D. Thesis, MIT Artificial Intelligence Laboratory, 1988.

[8] D. Borro, J. Savall, A. Amundarain, J. J. Gil, A. García-Alonso, and L. Matey, "A large haptic device for aircraft engine maintainability," *IEEE Comput. Graph. Appl.*, vol. 24, no. 6, pp. 70–74, 2004.

[9] J. Savall, D. Borro, A. Amundarain, J. Martin, J. J. Gil, and L. Matey, "LHIfAM – Large Haptic Interface for Aeronautics Maintainability," in *IEEE Int. Conf. Robot. Autom.*, ser. Video Proceedings, New Orleans, Louisiana, USA, 2004.

[10] J. J. Gil, A. Avello, A. Rubio, and J. Flórez, "Stability analysis of a 1 dof haptic interface using the routh-hurwitz criterion," *IEEE Trans. Control Syst. Technol.*, vol. 12, no. 4, pp. 583–588, 2004.

[11] K. J. Kuchenbecker and G. Niemeyer, "Modeling induced master motion in force-reflecting teleoperation," in *IEEE Int. Conf. Robot. Autom.*, Barcelona, Spain, 2005, pp. 350–355.

[12] J.-H. Ryu, C. Preusche, B. Hannaford, and G. Hirzinger, "Time domain passivity control with reference energy following," *IEEE Trans. Control Syst. Technol.*, vol. 13, no. 5, pp. 737–742, 2005.

[13] K. J. Aström and T. Hägglund, *PID Controllers: Theory, Design, and Tuning*. North Carolina: Instrument Society of America, 1995.

[14] L. Barbé, B. Bayle, and M. de Mathelin, "Towards the autotuning of force-feedback teleoperators," in *8th International IFAC Symposium on Robot Control*, Bologna, Italy, September 6-8 2006.

[15] R. J. Adams and B. Hannaford, "Stable haptic interaction with virtual environments," *IEEE Trans. Robot. Autom.*, vol. 15, no. 3, pp. 465–474, 1999.